13.4 ENVIRONMENTAL ATMOSPHERIC CONDITIONS UNDER WHICH A TORNADO FORMED OVER HOKKAIDO ISLAND, JAPAN ON 7 NOV. 2006, DETECTED FROM A SUPERCELL REPRODUCED BY A CLOUD-RESOLVING MODEL

Teruyuki KATO* and Hiroshi NIINO**

*Meteorological Research Institute, Tsukuba, Ibaraki, Japan

**Ocean Research Institute, The University of Tokyo, Nakano, Tokyo, Japan

1. INTRODUCTION

A tornado occurred in the northeastern part of Hokkaido Island, the north part of the Japan Islands, at 1325JST (JST=UTC+9hours) on 7 November 2006. The occurrence point of the tornado is marked with **x** in Fig. 1d. Nine persons were killed, which is the worst death toll due to a tornado in Japan since 1942.

In the present study, environmental atmospheric conditions under which the supercell causing the tornado formed are examined from observed data, objective analysis data and successful simulation results of a cloud-resolving model (CRM) with the horizontal resolution of 1 km (1km-CRM). Conventional meteorological radar data and surface observation data, operationally obtained by the Japan meteorological Agency (JMA), are used. The upper air conditions are examined mainly by using the successfully reproduced results of the 1km-CRM, since the temporal and spatial resolutions of the existing upper air soundings are not sufficient to represent the environmental conditions of the storm that spawned the tornado.

Moreover, the structure of the storm that caused the tornado and the formation factors of the tornado are also investigated using a cloud-resolving model with the horizontal resolution of 250 m (250m-CRM).

* *Corresponding author address:* Teruyuki Kato, Meteorological Research Institute, 1-1 Nagamine, Tsukuba, Ibaraki 305-0035 JAPAN; e-mail: tkato@mri-jma.go.jp.

2. NUMERICAL MODELS

Three numerical models used in the present study are all based on the JMA-nonhydrostatic model (JMA-NHM, Saito et al., 2006). The same dynamical and physical processes but the precipitation and atmospheric boundary layer processes are used in the three numerical models: In the 1km-CRM and 250m-CRM, bulk-type microphysics scheme predicting the mixing ratios of cloud water, cloud ice, rainwater, snow, and graupel are used for the precipitation processes, while the moist convection parameterization scheme (Kain and Fritsch, 1990) is additionally used in the 5km-NHM. As for the atmospheric boundary layer processes, the 1km-CRM and 250m-CRM predict the turbulent energy (Deardroff, 1980), while the 5km-NHM prognostically estimates the turbulence energy and incorporates a mixing length formulation that supports a realistic boundary layer growth (Kumagai, 2004). The other configurations are almost the same as described in Saito et al. (2006).

The experimental design is shown in Fig. 1a. The initial and boundary conditions of 1km-CRM and 250m-CRM are produced by simply interpolating the predictions of a nonhydrostatic model with 5km-NHM and the 1km-CRM, respectively. Those of 5km-NHM are produced from 6-houly available mesoscale objective analysis data (MANAL) having a horizontal resolution of about 10 km. The initial times of 5km-NHM, 1km-CRM, and 250m-CRM are 09JST, 10JST, and 12JST on 7 November 2006, respectively.

The calculation domain for each model is respectively shown in Figs. 1b, 1c, and 1d. The domain

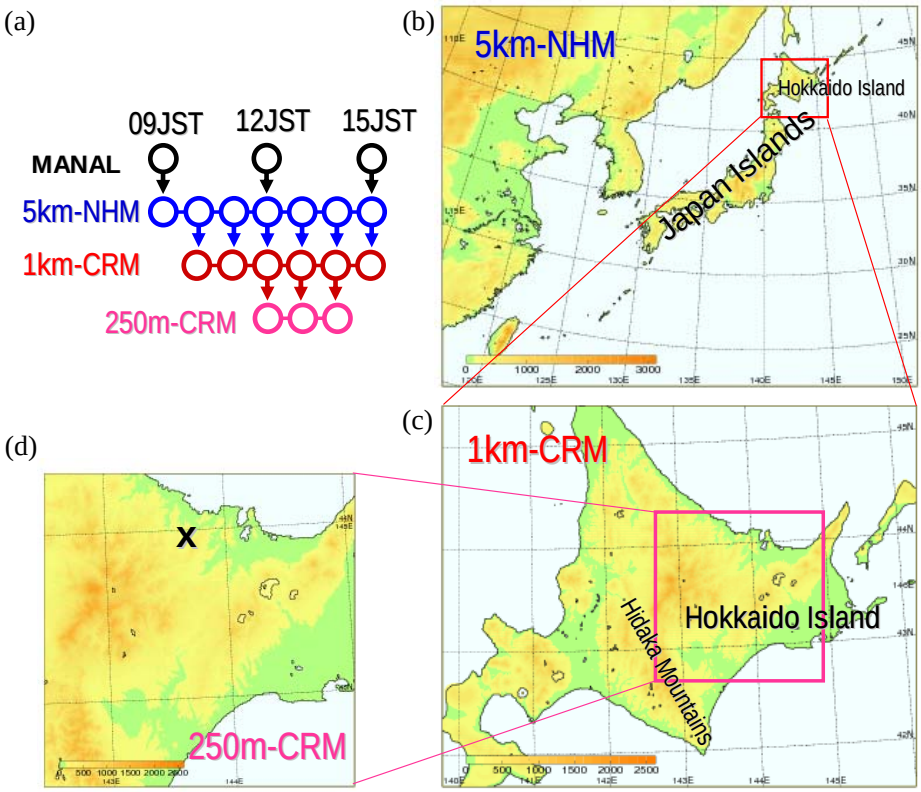

Fig. 1 (a) Experiment design: nesting procedure of 5km-NHM, 1km-CRM, 250m-CRM. MANAL is the mesoscale analysis operationally produced by the JMA. Model domain and topography of (b) 5km-NHM, (c) 1km-CRM, and (d) 250m-CRM. The occurrence point of the tornado is marked with **x** in (d).

size of the 5km-NHM is 3500 km x 2900 km, covering all the Japan Islands, and that of the 1km-CRM is 500 km x 400 km, covering almost the area of Hokkaido Island. The domain of the 250m-CRM (200 km x 200 km) covers the area where the parent storm of the tornado traveled. The topography of each model is produced by averaging the GTOP30 (horizontal resolution: about 1 km) of U.S. Geological Survey. Therefore, the 250m-CRM expresses almost the same topography as that of 1km-CRM.

3. MOVEMENT OF THE CUMULONIMBUS CAUSING THE TORNADO AND SIMULATED RESULTS

The storm that spawned the tornado was initiated on the east flank of the Hidaka Mountain Range (see Fig, 1c) around 1120JST on 7 November. Figure 2a shows the time evolution of the precipitation intensity as estimated from radar observation at that time, while Fig. 2b that simulated by the 1km-CRM. The observed and simulated near-surface winds are also shown with arrows in Figs. 2a and 2b, respectively. The 1km-CRM well reproduces not only the rainfall distributions, but also the time and location of the initiation of the storm around 1120JST on the eastern flank of the Hidaka Mountain Range, Its traveling speed (about 80 km h^{-1}) and direction (north-northeast are also well reproduced. Moreover, the rainfall distribution of the storm right before the tornado occurred (at 1320JST) is preciously simulated by the 1km-CRM. It should also be noted that the near-surface wind distribution at 1120JST when the storm was initiated is also well reproduced

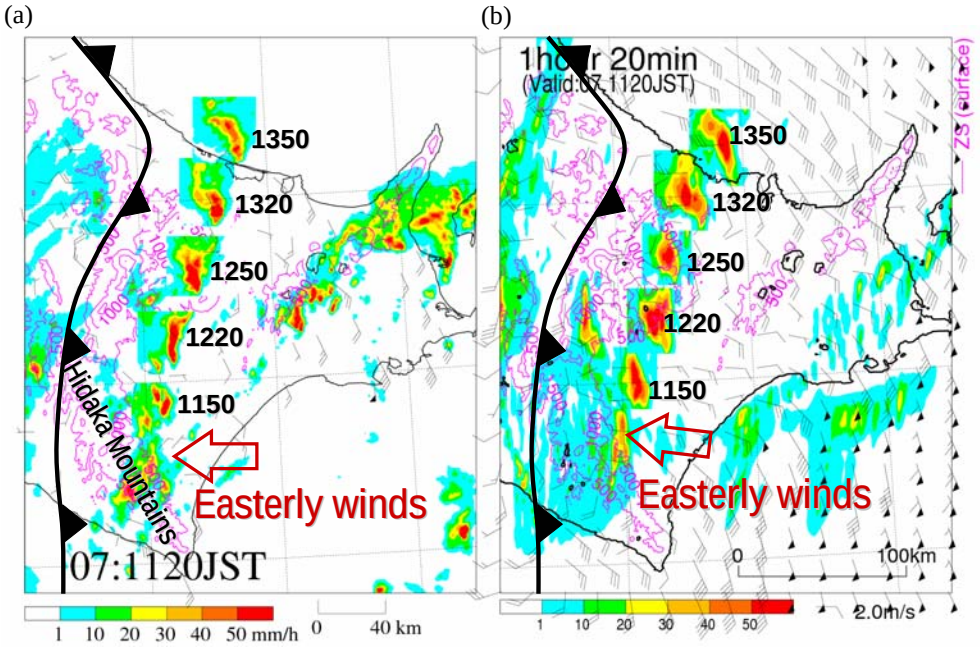

Fig. 2 (a) Distribution of precipitation intensity estimated from radar observation at 1120JST on 7 November 2006, and the movement of those associated with the cumulonimbus causing the tornado with an interval of 30 minutes. Arrows denote the observed near-surface winds, and pink-colored contours show the topography with an interval of 500 m. (b) Same as (a), but for the simulation results of the 1km-CRM.

These results show that the environmental atmospheric conditions are well reproduced by the 1km-CRM. Therefore, the environmental atmospheric conditions under which the storm spawning the tornado formed and developed will be hereafter examined based on the successful simulation results of the 1km-CRM

When the storm formed around 1120JST, a cold front extended southward from a developed extratropical cyclone north of Hokkaido Island, to the western side of the Hidaka Mountain Range (see Fig. 2a). Easterly winds prevailed in the lower atmosphere over the formation area of the storm (see Fig. 4), while strong southerly winds at the mid-level prevailed in the warm sector of the extratropical cyclone. The wind hodograph (Fig. 4a) shows a clockwise rotation of the wind vector with increasing height.

The time series of near-surface temperature, winds, and rainfall amount observed at Saroma 2 km east of the occurrence point of the tornado are shown in Fig. 3. The cold front passed this observation point at around 1500JST when the temperature dropped about 4 K.

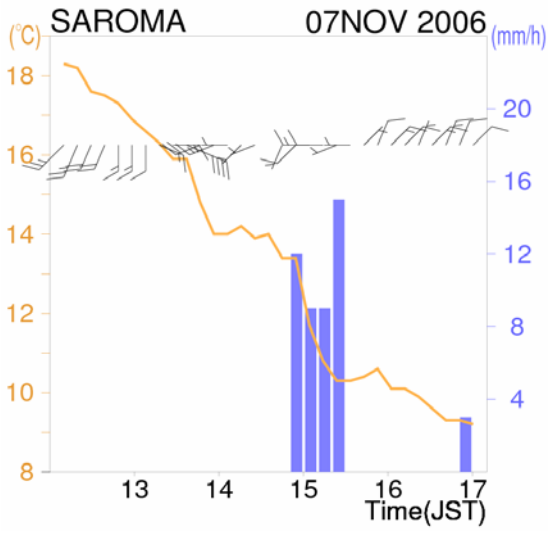

Fig. 3 Time series of temperature(orange line), winds (arrows), and precipitation intensity (blue bars) between 1200JST and 1700JST, observed about 2 km east of the occurrence point of the tornado.

Thus, the parent storm of the tornado traveled in the warm sector side of the cold front. It should be noted that high temperature exceeding 16 °C was maintained until the tornado occurred. The high temperature was caused by foehn phenomena, which will be examined in detail in Section 6.

4. ENVIRONMENTAL ATMOSPHERIC CONDITIONS FOR INITIATING AND MAINTAINING THE PARENT STORM OF THE TORNADO

First, the environmental wind conditions in which the parent storm of the tornado formed are examined. Figure 4a shows the vertical profile of 1km-CRM simulated winds at 1120JST at the point marked with **x** in Figs. 4b - 4d, which almost corresponds to the formation area of the storm. Low-level winds below 3-km above the ground level (AGL) have an easterly component due to the effect of the Hidaka Mountain Range. The wind vector rotates clockwise with the wind speed increasing with height. Note that the wind speed reaches about 60 m s^{-1} at 8km AGL. Such a vertical profile of wind is favorable for the formation of supercells with rotating updrafts.

The environmental winds at heights of 5km and 2km and the surface at 1120 when the parent storm of the tornado formed are shown in Figs. 4b – 4d. The low-level winds with an easterly component, found in Fig. 4a, are remarkably distributed on the northern side of the formation area of the storm (Fig. 4d). This characteristic feature is also found at a height of 2km, although the easterly component becomes weak (Fig. 4c). On the other hand, the easterly component of wind cannot be found at a height of 5km around the formation area of the storm (Fig. 4b). The region with an easterly component of wind is therefore limited to at the lower level on the northern side of the formation area of the storm.

In order to examine the time evolution of the environmental wind conditions, the storm-relative environmental helicity (*SREH*))

$$SREH = \int_0^{3km} \mathbf{k} \cdot (\mathbf{v} - \mathbf{c}) \times \frac{\partial \mathbf{v}}{\partial z} dz \quad ,$$

is calculated, where $\mathbf{c}$ is the traveling vector of storm, estimated from radar observations, and $\mathbf{v}$ is the horizontal wind vector. *SREH* is an index that measures the tendency of the storm updraft to have a rotation about the vertical axis. Davies-Jones et al. (1990) showed that a potential for the formation of supercells is extremely high for *SREH* > 500 m^2 s^{-2}.

Figure 5 shows the *SREH* distributions calculated from the simulation results of the 1km-CRM with a time interval of 30 min. At 1120JST, the *SREH* is larger than 700 m^2 s^{-2} around the formation area of the parent storm of the tornado (shown by a white cycle in the left panel of Fig. 5). This shows that not only the environmental condition is favorable, but also the storm itself modifies its environment favorable for the formation of supercells. After this time, area region with *SREH* > 1000 m^2 s^{-2} appears ahead of the storm and continues to move with the storm. This increase of *SREH* on the northern side of the storm is associated with the enhancement of the storm-induced easterly component of low-level winds. This enhancement of the easterly component was also observed by a wind profiler whose location is marked with **x** in the left panel of Fig. 5 (not shown).

The enhancement of the easterly component of winds on the northern side of the storm is related to the storm-induced pressure field: A remarkable pressure drop of about 2 hPa is continuously found at the low-level ahead of the storm (not shown). The pressure gradient force associated with that pressure drop over 50 km is about 2 m s^{-1} / 10 min and seems to be responsible for the enhancement of the easterly component of winds.

Next, the thermodynamic features of the environmental atmospheric conditions for the storm are examined using the simulation results of the 1km-CRM. Color shade in Figs. 4b – 4d shows the distance between the originating level of lifting air and the level of free convection *dLFC*, the convective available potential energy *CAPE*, and the level of neutral buoyancy *LNB*. The originating level of lifting air is determined from the

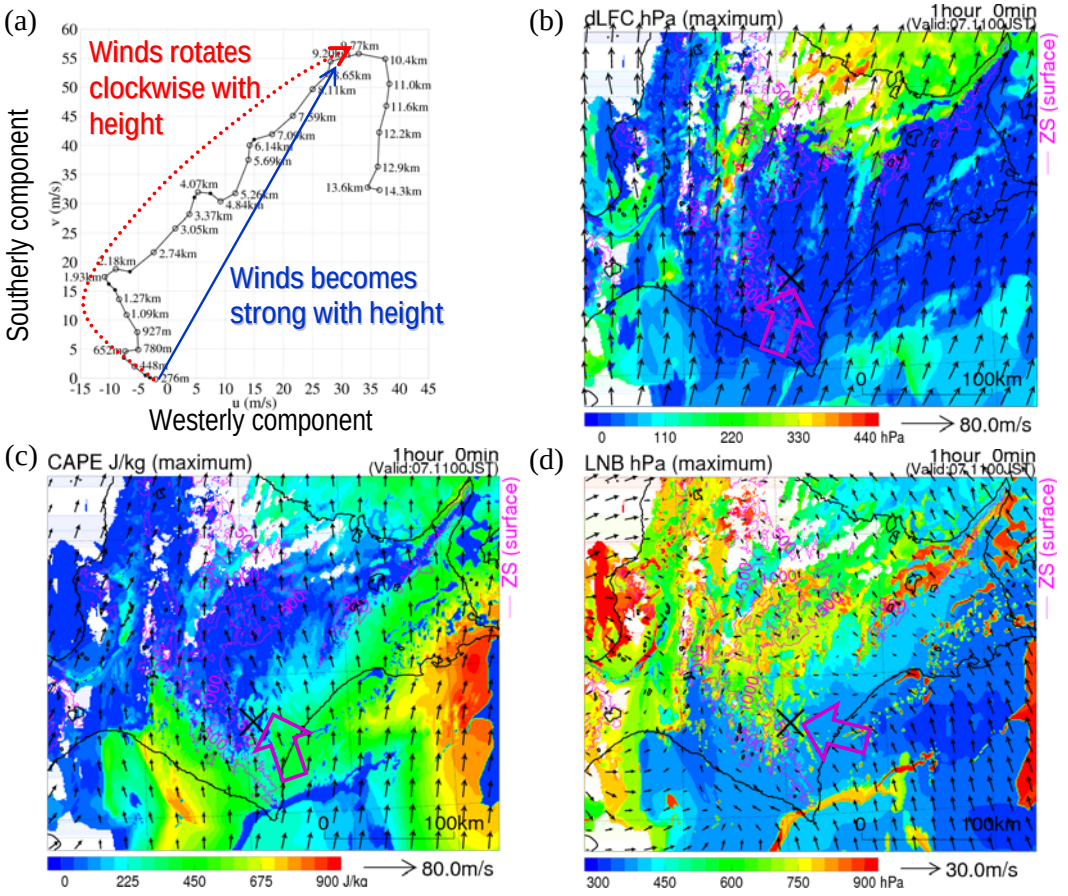

Fig. 4 (a) Vertical profile of 1km-CRM simulated winds at 1100JST on 7 November 2006 at the point marked with **x** in (b) – (d). (b) Distance between the originating level of lifting air and the level of free convection *dLFC*, (c) convective available potential energy *CAPE*, and (d) the level of neutral buoyancy *LNB* at 1100JST, calculated from the simulation results of the 1km-CRM. The originating level of lifting air is determined from the maximum equivalent potential temperature below an 800-hPa level. Vectors in (b), (c) and (d) denote the simulated winds at heights of 5 km, 2 km, and near the surface, respectively.

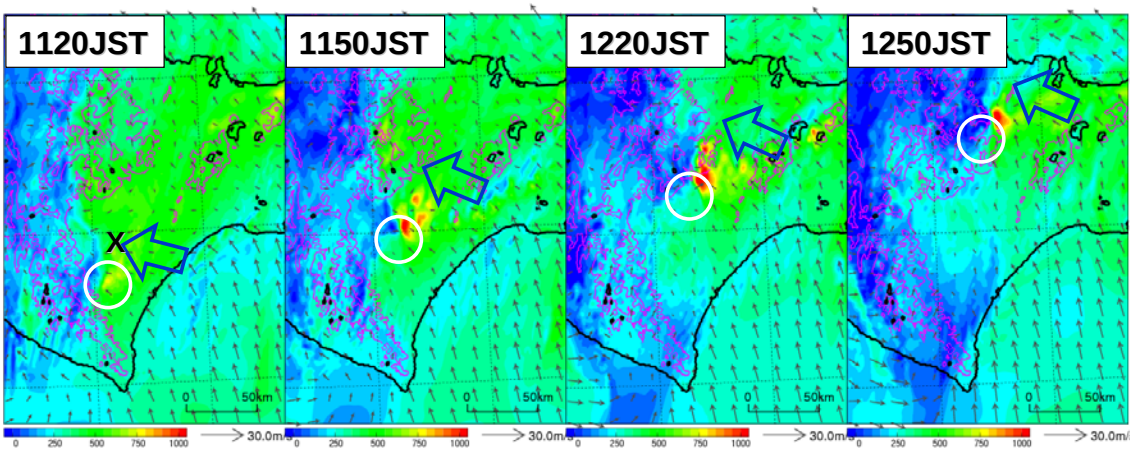

Fig. 5 Distribution of *SREH* (m^2 s^{-2}) at 1120JST, 1150JST, 1220JST and 1250JST, calculated from the simulation results of the 1km-CRM. Vectors denote simulated near-surface winds.

maximum equivalent potential temperature θ_{emax} below an 800-hPa level.

The *dLFC* around the formation area of the parent storm of the tornado, marked with **x** in Figs. 4b, is very small (< 50 hPa), suggesting a favorable atmospheric condition for a storm formation. *CAPE* is less than 400 J kg^{-1} there (Fig. 4c), and is considerably smaller than typical values for supercells in the central part of the United States (~ 2000 J kg^{-1}). Since heavy rainfall is often observed in Japan for small *CAPE* (~ 500 J kg^{-1}), however, *CAPE* alone is not a suitable for judging a potential for a severe phenomena (e. g., Kato and Goda, 2001). *LNB* is about 350 hPa around the formation area of the storm. This level is consistent with the cloud top height observed by a JMA radar (8 ~ 10 km), because updrafts could reach slightly higher than the *LNB*.

A sustained inflow of humid air with high θ_e is necessary for the maintenance of convective activities. The southerly component of wind speed is less than 10 m s^{-1} below a 1-km height (Fig. 4a). This means that humid air was never supplied from the south into the storm, because its traveling speed was about 20 m s^{-1} in the northward direction.

Figure 6 shows the distributions of the maximum equivalent potential temperature θ_{emax} below 800hPa at a time interval of 30min, where θ_{emax} has been calculated from the simulation results of the 1km-CRM. At 1120JST, southerly winds were bringing high θ_e air from the sea area south of Hokkaido Island, and a region with remarkable gradient of θ_e is found from the formation area of the storm to a north-northeast direction (left panel of Fig. 6). The region having an extremely strong gradient of θ_e propagates northward with time, and consequently high θ_e air continued to exist on the eastern side of the storm. Moreover, the enhancement of the easterly component of winds on the northern side of the storm played a significant role on the further transport of high θ_e air to the west. As mentioned above, the parent storm of the tornado maintained the favorable environmental atmospheric conditions for convective activities by itself.

5. STRUCTURE OF THE PARENT STORM OF THE TORNADO

Figure 7a shows the distribution of precipitation intensity estimated from radar observation and the near-surface winds at 1320JST right before the tornado was observed. The radar observation shows that the occurrence point of the tornado, marked with a solid cycle in Fig. 7a, is located on the eastern side of the area with strong precipitation. It is seen that the surface observation stations are so sparse that no indication of a tornado is found. A detailed distribution of winds is examined by using the simulated results of the 250m-CRM (Fig. 7b), accordingly.

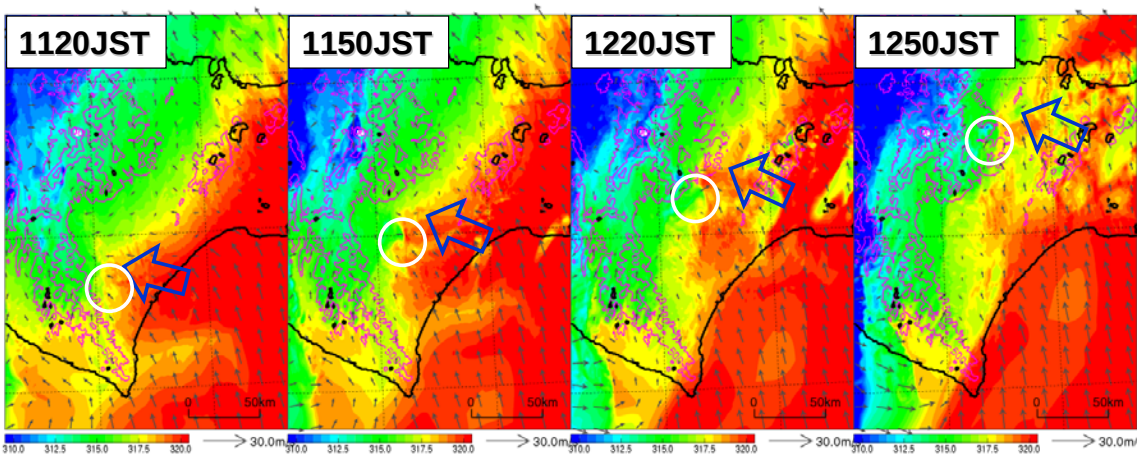

Fig. 6 Same as Fig. 5, but for the maximum equivalent potential temperature below an 800-hPa level.

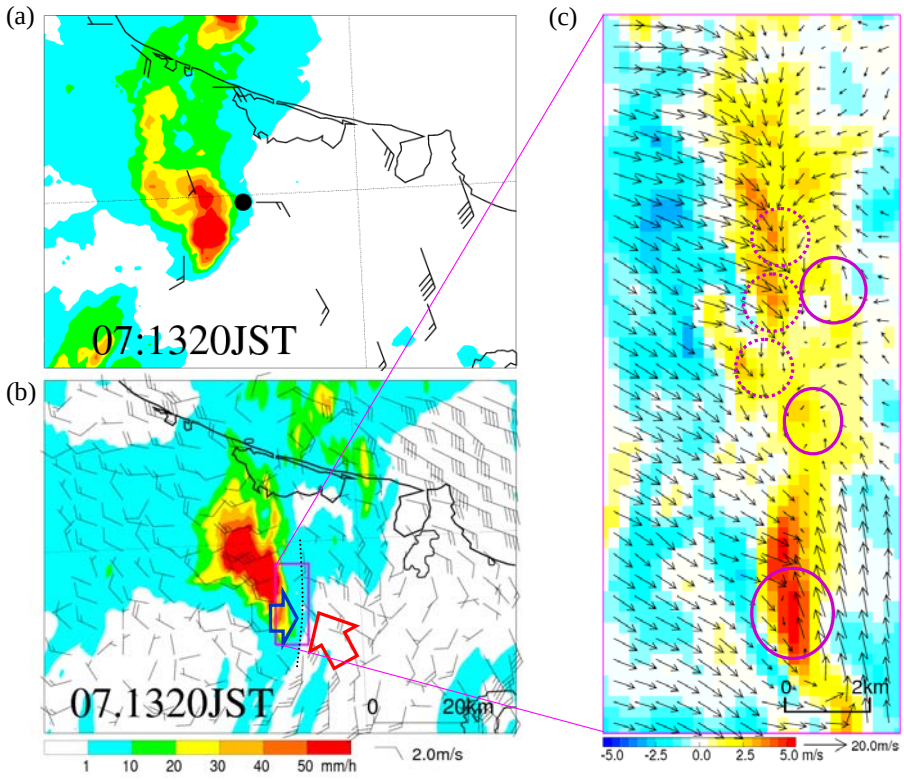

Fig. 7 (a) Distribution of precipitation intensity estimated from radar observation and the near-surface observed winds at 1320JST. Filled black cycle denotes the occurrence point of the tornado. (b) Same as (a), but for the simulation results of the 250m-CRM. (c) Distribution of simulated winds (vectors) and vertical velocity (colored shade) at a 300-m height from the ground within the pink-colored rectangle in (b). Here, wind vectors are drawn decreasing the northward component of wind speed by 8 m s^{-1} to easily district vortexes.

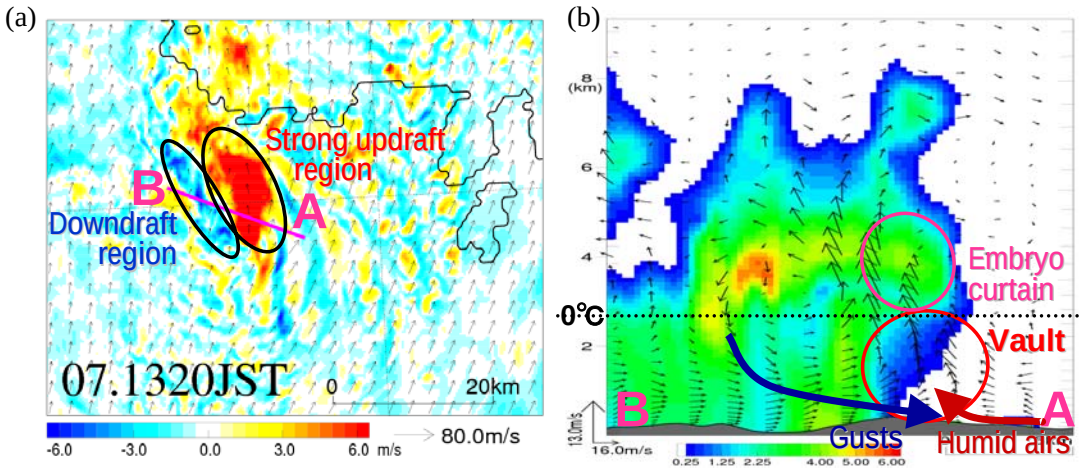

Fig. 8 (a) Distribution of 250m-CRM simulated vertical velocity (colored shade) and winds (vectors) at 1320JST. (b) Vertical cross section of precipitation material (rain + snow + graupel) along the line AB in (a). Vectors denote winds projected on this vertical cross section.

The simulated rainfall distribution associated with the storm well reproduces the radar observation except that its location is about 10 km east of the observation. The wind distribution shows that the cold-air flow produced in the storm (indicated by the black arrow in Fig. 7b) collides with the low-level inflow of humid and warm air (indicated by the red arrow) on the southeastern side of rainfall area, and forming a gust front.

Figure 7c shows the distribution of simulated horizontal winds and vertical velocity at 300m AGL around the gust front (pink-colored rectangle in Fig. 7b). Here, wind vectors are drawn after subtracting 8 m s^{-1} from the northward component of wind speed in order to easily recognize the existence of vortices. Several anti-clockwise vortices with significant vertical vorticity (indicated by pink-colored cycles), are found over the gust front. Any of them may become a tornado if vertically stretched by a strong updraft above.

Next, the inner structure of the parent storm of the tornado is examined using the simulated results of the 250m-CRM. Figure 8a shows the distribution of vertical velocity w at a height of 3km at 1320JST right before the tornado was observed. A region of strong updraft exceeding 6 m s^{-1} (the maximum w is about 15 m s^{-1}) extends over 20 km in a south-north direction, while a region of remarkable downdraft exist on the western side. This pair of strong updraft and downdraft regions continuously existed right after the formation of the storm. A region of positive vorticity exceeding 10^{-2} s^{-1} is also found on the region of the strong updraft region. Therefore, the simulated storm satisfies the criterion of a supercell.

Figure 8b shows the vertical cross section of precipitation substance (rainwater + snow + graupel) along line AB in Fig. 8a. A precipitation-free vault is found at the lower level in the strong updraft region. Right above the vault, an embryo curtain, an area where graupel and hail form and develop, exists. In the present simulation, most of hydrometeors in the area are graupel. Note that a category of hail is not considered in the JMA-NHM, although hail was observed in association with the storm.

Simulated precipitation at the ground is found on the western side of the strong updraft region, and the water loading effect due to the precipitation causes downdrafts there. A cold outflow originated from the downdrafts produce the gust front by colliding with the southerly inflow of humid and warm air into the low-level of the storm. These features demonstrate that the simulated storm had characteristics of a supercell. The parent storm of the tornado is hereafter referred to as “the supercell”, accordingly.

6. FORMATION FACTORS OF THE TORNADO

Tornados are often observed along a gust front associated with supercells. In the present case, however, only one tornado was observed in the life cycle of the supercell, i.e., for about two hours after the formation of the supercell. Therefore, the factors to cause the tornado when the supercell arrived at the northern part of Hokkaido Island are examined.

Figure 9 shows the distributions of radar estimated precipitation intensity and observed near-surface temperature and winds at 1200JST. The rainfall associated with the supercell is marked with a black circle in Fig. 9. The temperature of the air flowing from the south of Hokkaido Island was 14 ~ 15 °C, while that around the tornado occurrence exceeded 18 °C. Here, it should be noted that rainfall was observed over the mountains with a height of 500 ~ 1500 m, marked with a blue ellipse shown in Fig. 9. This rainfall indicates that southerly winds caused foehn phenomena around the area of the tornado occurrence.

The foehn phenomena continued to occur until the passage of the supercell (see Fig. 3): the high temperature above 14 ~ 15 °C in Fig. 3 before 1340JST is caused by the foehn phenomena. The relative humidity is lower in the area around the tornado occurrence, which is consistent with the foehn phenomena. Note that the foehn phenomena never change the LFC because of the conservation of θ_e, although cloud-base heights become higher due to the lowering of relative humidity.

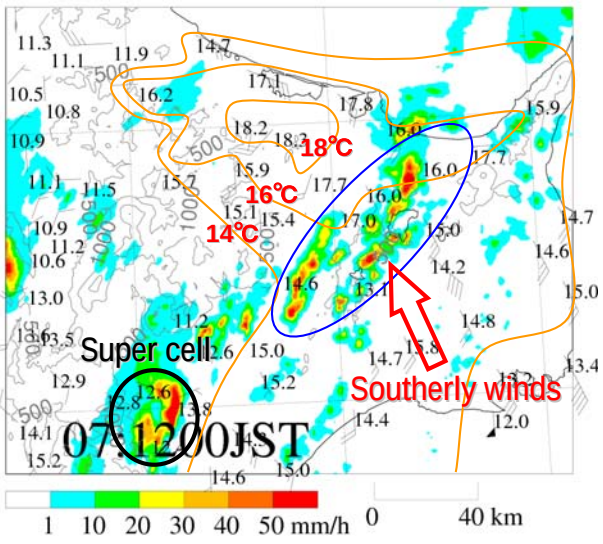

Fig. 9 Distribution of radar-estimated precipitation intensity (colored shade) and the observed near-surface temperature distribution (orange contours) and winds (arrows) at 1200JST.

The reproductivity of the foehn phenomena in the simulation results of the 1km-CRM is ascertained. Figure 10 shows the near-surface distribution of simulated temperature and relative humidity at 1300JST. The higher temperature and lower relative humidity around the area of the tornado occurrence are well reproduced.

The height of the layer influenced by the foehn phenomena is examined next.

Figure 11 shows the vertical profile of potential temperature near the area of the tornado occurrence , indicated by **x** in Fig. 10, at 1300JST. A dry layer affected by the foehn phenomena is found below a height of 1 km, where the difference between the θ_e and the saturated equivalent potential temperature θ_e^* is large. Above this layer the atmosphere is almost saturated, because humid air contaminated with snow produced in the supercell, was advected by upper strong winds ahead of the supercell (not shown). This indicates that an intrusion of middle-level air into the supercell to cause an enhancement of downdrafts was not possible, because little evaporation of precipitation material is expected above a height of 1 km. However, significant evaporation of raindrops could have occurred when they fall into the dry layer below a height of 1 km, and may have enhanced downdrafts and gusts. This is ascertained from the simulation results of the 250m-CRM.

The decrease of simulated temperature for 20 min from 1320JST on the western side of the gust front is about 2 K (not shown). The pressure gradient force between the meso high produced by this cooling and the meso low found on the eastern side of rainfall area (not

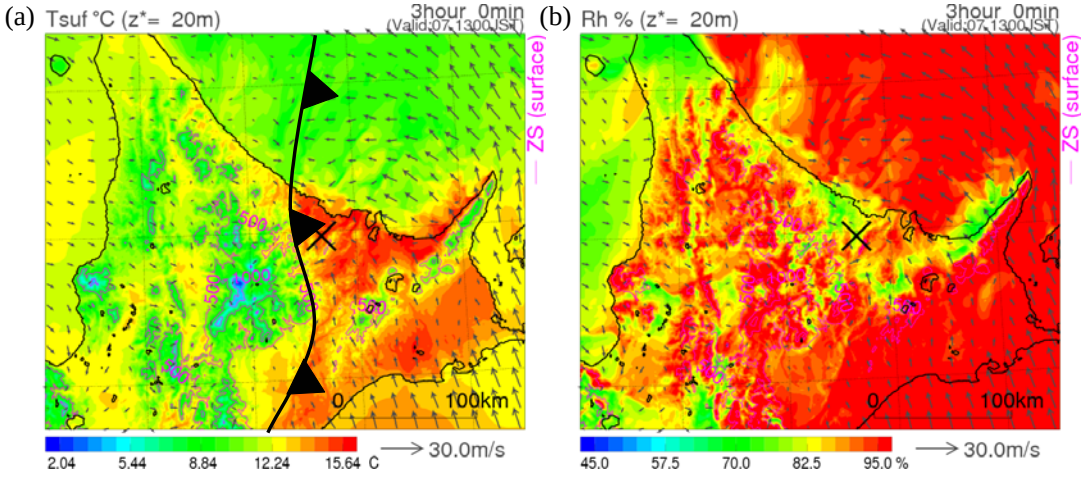

Fig. 10 Distributions of 1km-CRM simulated (a) temperature and (b) relative humidity at a height of about 20 m from the ground at 1300JST. Vectors denote simulated winds.

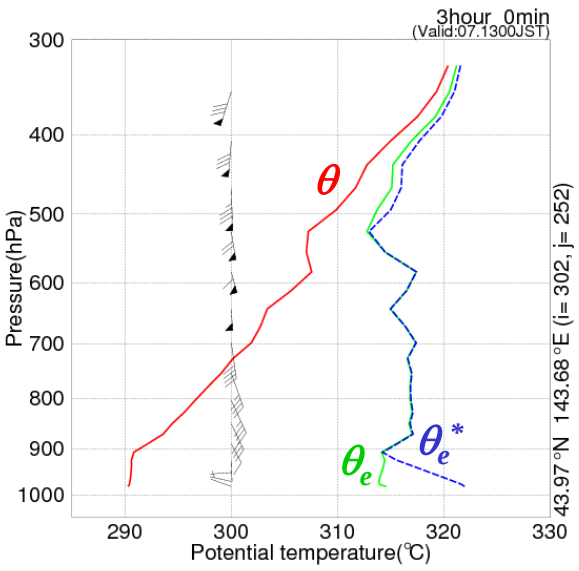

Fig. 11 Vertical profiles of 1km-CRM simulated potential temperature θ, equivalent potential temperature θ_e, and saturated equivalent potential temperature θ_e^* at 1300JST at the point marked with **x** in Fig. 10.

shown) further enhanced the gusts. Figure 12a shows the distribution of the westerly component of simulated winds at 200m AGL at 1320JST. Strong westerly winds exceeding 15 m s^{-1} are found on the western side of the gust front. In order to examine the influence of foehn phenomena on the production of the strong winds, a sensitive experiment in which the evaporation of raindrops is suppressed below about 1.5 km AGL was performed. The result of the sensitive experiment is shown in Fig. 12b. The gusts became weaker by 2 ~ 3 m s^{-1} than those in the control experiment (Fig. 12a). This is because the decrease of simulated temperature for 20 min on the western side of the gust front is reduced to less than 1 K (not shown). Also performed was another sensitive experiment in which the evaporation of all precipitation material is suppressed in whole the model domain. Its results were nearly same as those of the first sensitive experiment (Fig. 12b). This shows that the intrusion of middle-level air into the supercell hardly contribute to the enhancement of downdrafts.

These results suggest that the following factor were important for causing the tornado. 1) The lower atmosphere becomes dry due to foehn phenomena. 2) Gusts are enhanced by the evaporation of raindrops in the dry layer. 3) Consequently, the convergence of winds over the gust front becomes larger, and the vertical vorticity also becomes larger there. This large vertical vorticity is stretched by updrafts associated with the supercell, and the tornado could form.

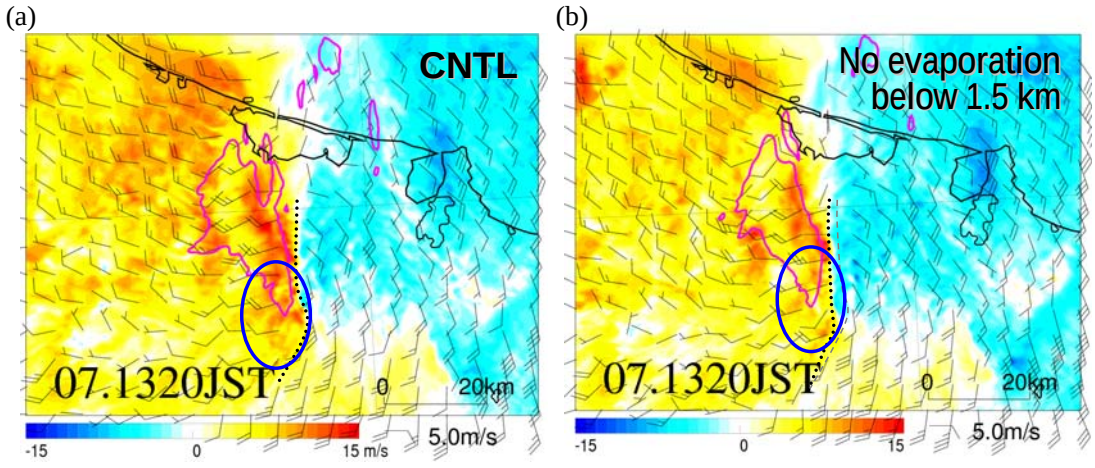

Fig.12 Distribution of the westerly component of 250m-CRM simulated winds at 1320JST at a height of about 200 m from the ground in (a) the control experiment and (b) the sensitive experiment without the evaporation of raindrop below a height of about 1.5 km.. Arrows denote simulated winds.

Another factor to cause the tornado could be examined. Figure 13 shows the detail topography around the occurrence point of the tornado. The observed position of the tornado, marked with **x** in Fig. 14, located just in the open area of two valleys with a depth higher than 500 m. Over such a location, even the uniform flow can produce the vertical vorticity due to the effect of topography. This effect could enhance the vertical vorticity over the gust front.

7. SUMMARY AND FUTURE ISSUES

Environmental atmospheric conditions under which a tornado occurred in the northeastern part of Hokkaido Island, the north part of the Japan Islands, on 7 November 2006 are examined from observed data, objective analysis data and successful simulation results by a cloud-resolving model with the horizontal resolution of 1 km (1km-CRM). The structures of the supercell causing the tornado and the formation factors of the tornado are also investigated using a cloud-resolving model with the horizontal resolution of 250 m (250m-CRM).

The simulated supercell has the height of about 10 km, the width of 20 ~ 30 km, and such characteristic features of classical supercells as a pair of strong rotating updraft and remarkable downdraft regions, “vault” and “embryo curtain”. The supercell formed on the eastern flank of the Hidaka Mountain Range, the northeastern part of Hokkaido Island. The vertical wind conditions there are favorable for the formation of supercells, i.e., the vertical profile of winds had the easterly component at the lower level, and rotated clockwise and became stronger with increasing height. Moreover, the supercell maintained such favorable wind conditions by itself with traveling north-northeastward. Further, before the formation of the supercell southerly winds transported low-level humid airs into the inland of Hokkaido Island, and the supply of the airs maintained convective activities of the supercell.

Fig. 13 Topography around the occurrence point of the tornado.

When the supercell arrived at the northeastern part of Hokkaido Island after about two hours from its formation, the tornado occurred there. Southerly winds flew over the mountains with a height of 500 ~ 1500 m, located south of the occurrence point of the tornado, and they caused foehn phenomena. The foehn phenomena made the atmospheric condition dry at the lower level, and it could be one of the factors to cause the tornado. The results of sensitive experiments show that the gusts from the supercell are enhanced by the evaporation of raindrops in the lower layer. The gusts and the southerly inflow of humid airs into the supercell produce the gust front, and one of vortexes over the gust front could be stretched upward to become the tornado. Moreover, another factor to cause the tornado could be the effect of topography around the occurrence point of the tornado.

Since the 250m-CRM can not reproduce tornadoes due to the rough resolution, the CRM with the finer resolution is necessary to do so. The study using such a CRM is in our future issues. In them, the effect of topography is also examined through sensitive experiments.

References

Davies-Jones, R., D. Burgess, and M. Foster, 1990: Test of helicity as a tornado forecast parameter. *16th Conf. on Severe Local Storms, Oct. 22-26, 1990, Kananaskis Park, Alta, Canada, Amer. Meteor. Soc.*, 588-592.

Deardorff, J. W., 1980: Stratocumulus-capped mixed layers derived from a three-dimensional model. *Bound.-Layer Meteor*., **18**, 495–527.

Kain, J. S. and J. M. Fritsch, 1990: A one-dimensional entraining/detraining plume model and its application in convective parameterization. *J. Atmos. Sci.*, **47**, 2784-2802.

Kato, T. and H. Goda, 2001: Formation and maintenance processes of a stationary band-shaped heavy rainfall observed in Niigata on 4 August 1998. *J. Meteor. Soc. Japan,* **79**, 899-924.

Kumagai, Y., 2004: Implementation of a non-local like PBL scheme in JMANHM. *CAS/JSC WGNE Res. Activ. Atmos. Oceanic Modell*., **34**, 0417–0418.

Saito, K, T. Fujita, Y. Yamada, J. Ishida, Y.Kumagai, K. Aranami, S. Ohmori, R. Nagasawa, S. Kumagai, C. Muroi, T. Kato, H. Eito, and Y. Yamazaki, 2006: The Operational JMA Nonhydrostatic Mesoscale Model, *Mon. Wea. Rev*., **134,** 1266-1297.